Experimental and theoretical studies of active control of resistive wall mode growth in the EXTRAP T2R reversed-field pinch

J.R. Drake 1), P.R. Brunsell 1), D. Yadikin 1), M. Cecconello 1), J.A. Malmberg 1), D. Gregoratto 2), R. Paccagnella 2), T. Bolzonella 2), G. Manduchi 2), L. Marrelli 2), S. Ortolani 2), G. Spizzo 2), P. Zanca. 2), A. Bondeson 3), Y.Q. Liu 3)

1) Alfvén Laboratory, KTH, EURATOM VR Association, Stockholm, Sweden
2) Consorzio RFX, EURATOM ENEA Association, Padova, Italy
3) Dept. of Electromagnetics, CTH, EURATOM Association VR, Gothenburg, Sweden
e-mail contact of main author: james.drake@alfvenlab.kth.se

Abstract. Active feedback control of resistive wall modes (RWMs) has been demonstrated on the EXTRAP T2R reversed-field pinch experiment. The control system includes a sensor consisting of an array of magnetic coils (measuring mode harmonics) and an actuator consisting of a saddle coil array (producing control harmonics). Closed-loop (feedback) experiments using a digital controller based on a real time Fourier transform of sensor data have been studied for cases where the feedback gain was constant and real for all harmonics (intelligent-shell) and cases where the feedback gain could be set for selected harmonics, with both real or complex values (targeted-harmonics). The growth of the dominant RWMs can be suppressed by feedback for both the intelligent-shell and targeted-harmonic control systems. Because the number of toroidal positions of saddle coils in the array is half the number of sensors, it is predicted and observed experimentally that the control harmonic spectrum has sidebands. As a result, each control harmonic has to control simultaneously two mode harmonics. Real gains can stabilize non-rotating RWMs, while complex gains give better results for (slowly) rotating RWMs. In addition open loop experiments have been used to observe the effects of resonant field errors applied to unstable, marginally stable and robustly stable modes. The observed effects of field errors are consistent with the thin-wall model, where mode growth is proportional to the resonant field error amplitude and the wall penetration time for that mode harmonic.

1. Introduction

Control of resistive wall modes (RWMs) is important for long pulse operation in reversed-field pinches (RWMs are $m=1$ current-driven, non-resonant, ideal kinks) and for achieving beta above the no-wall limit in advanced tokamaks (RWMs are $n\neq0$ pressure-driven external kinks). According to the thin-wall model if the wall is resistive and lies within the position for ideal wall stabilization, the kink modes develop as RWMs with growth rates of the order of the wall penetration time [1]. The EXTRAP T2R reversed-field pinch (RFP) has a thin shell (resistive wall) with a vertical magnetic field ($m=1,n=0$) penetration time of $\tau_w=6$ ms and has previously been used for experimental studies of the stability of RWMs [2, 3]. The focus of the program has now turned to development of methods for active feedback control the RWMs.

The system for active control of RWMs installed on T2R includes the following:

- A full-coverage, radial-field sensor coil array located just inside the shell that is 64 (toroidal) by 4 (poloidal) and series-connected to form an inboard-outboard pair (horizontal $m=1$ component) and top-bottom pair (vertical $m=1$ component). Mode harmonics can be resolved offline for $m=1$ modes in the range $-32\leq n\leq31$, while the digital controller makes use of the signals of only $N_s=32$ sensors in the toroidal direction, resolving modes in the range $-16<n<15$.

- A 50% coverage saddle coil array located just outside the shell that is 16 (toroidal) by 4 (poloidal) and series connected to form inboard-outboard and top-bottom pairs. The saddle coil width is twice the sensor coil width. Control harmonics can be produced for targeted m=1 modes in the range $-8 \leq n \leq 7$ with sidebands at Δn=16 intervals. For example targeting n=+5 also produces sideband harmonics at n=-11 and n=+21. The saddle coils are powered by suitably modified audio amplifiers. The maximum amplitude of the control field is of the order of one percent of the typical equilibrium field at the plasma edge, *i.e* 1 mT.
- A digital controller that generates the required waveform for the currents in the different saddle coils in the array needed to produce the specified control field harmonics. The controller can be used in a feedback system and in open-loop studies where the control field harmonic waveform is pre-programmed.

In the experiments, standard discharges are used. As shown in Ref. 3, in the RFP, the RWM spectrum and growth rates are dependent on the current profile, which in turn is dependent on the standard RFP equilibrium parameters. Three types of experiments have been carried out, intelligent-shell closed-loop control, targeted-mode closed-loop control and open-loop experiments to study resonant field error effects.

2. Feedback control experiments

The digital controller is a prototype of the controller developed for the RFX device at Padova [4]. In the feedback mode, the controller performs a real time FFT on the sensor coil data and utilizes a feedback law to determine the control harmonics. An inverse FFT yields the corresponding distribution of control signals required to steer the individual currents to the saddle coils in the array. The digital controller has been operated as an intelligent shell controller, where the feedback law has the same gain for each harmonic, and as a targeted-mode controller, where the feedback law has different gains for different modes.

Since the number of active coils is half the number of sensor coils, it is not possible to independently control each of the resolved field harmonics, i.e. the harmonics are coupled in pairs by the control system, b_{n1} and b_{n2} with $|n1\text{-}n2|$=16. Each control harmonic is then determined by a feedback law, which, for example in the case of current control, is $I_n = -K_{n1} b_{n1} - K_{n2} b_{n2}$, with appropriate gains K.

Examples of toroidal mode spectra of the radial field perturbation without feedback control and with intelligent shell feedback control are shown in FIG. 1. In the notation often used for the RFP, a negative toroidal mode number corresponds to the helicity handedness of the field inside the reversal surface, thus the tearing modes have m=1 and $n<-2R/r_w$. The m=1 non-resonant ideal modes that can potentially develop as RWMs or be affected by resonant field errors are either internally non-resonant ($-2R/r_w<n<0$) or externally non-resonant ($0<n$). Note in FIG. 1a that n=-12 is the first resonant surface located near the axis. The resonant tearing modes with $n \leq -12$ are rotating and as a result the radial field perturbations of these modes are low. The externally and internally non-resonant RWM modes are evident. The spectrum of the amplitudes is in rough agreement with the

theoretical growth rates but the n=-8 mode and the low $|n|$ modes clearly have exceptionally high amplitudes. The large amplitudes are attributed to resonant field error effects. Field errors are due to asymmetries in the external magnetic systems and the shell.

As seen in the spectrum shown in FIG. 1b, the intelligent shell feedback system reduces the amplitudes of the non-resonant modes. However the side-band effect causes a problem. Specifically, the side bands for the field error amplified modes in the range $-2 \leq n \leq 2$ are in the range $-18 \leq n \leq -14$, which corresponds to resonant tearing modes. The n=-14 side band produced by the controller when suppressing the n=+2 mode is an n=-14 perturbation, in effect a field error, that wall-locks the n=-14 tearing mode (note arrows in FIG. 1b). When the tearing modes wall-lock, the stabilising effect of rotation is lost and radial perturbation starts to grow which leads to termination of the discharge.

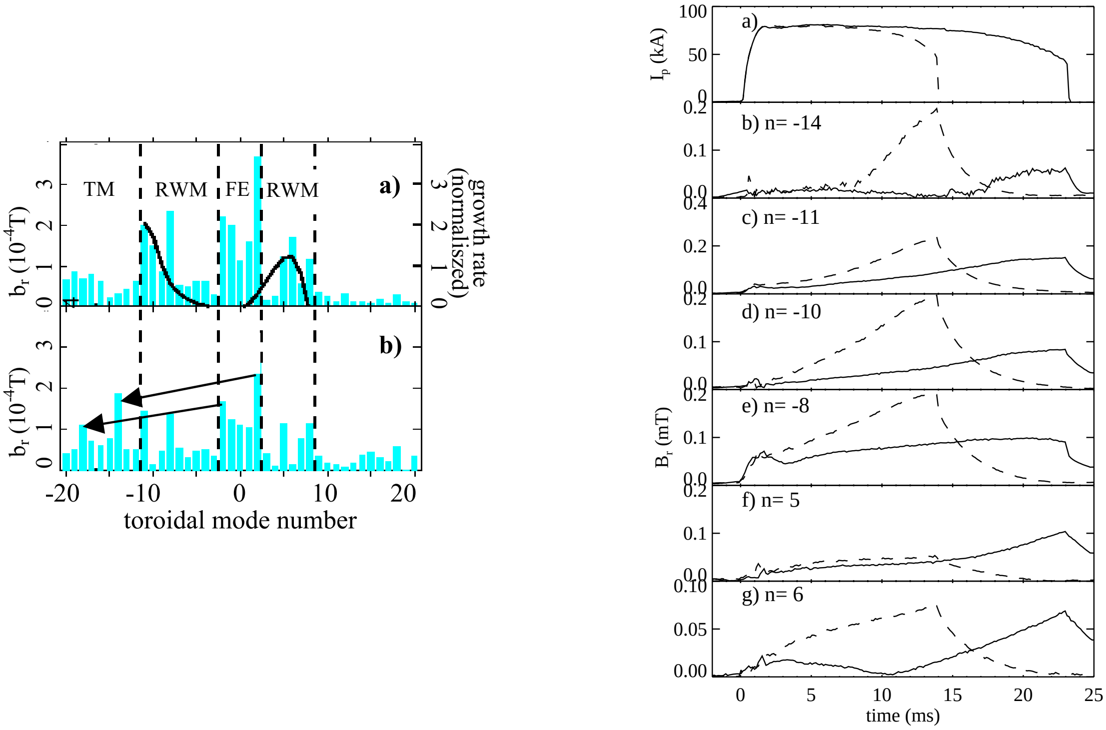

FIG. 1. On the left-hand side of the figure, panel (a) shows the m=*1 mode amplitudes for* n *in the range -20≤*n*≤+20 for a discharge without active feedback control at a time equal to 1.5 shell penetration times. The range includes internally resonant tearing modes (TM), RWMs and field error (FE) stimulated modes. The solid curve shows theoretically calculated normalised growth rates for the RWMs. In panel (b) the amplitudes for the same modes are shown with intelligent-shell active feedback in operation. On the right-hand side of the above figure, the time evolution of the discharge current and the harmonic amplitudes are shown for shots without (dashed line) and with (full line) targeted-mode feedback with gains corresponding to the intelligent shell case except that for modes* |n|*≤2 the gains are set equal zero. The* n=*-14 resonant tearing mode, the* n=*-11, -10 and –8 internally non-resonant RWMs and the* n=*+5 and +6 externally non-resonant RWMs are shown.*

This problem is partially alleviated for this special situation by using targeted-mode feedback, which utilises the capability for variable gains for different modes. When the controller is programmed so that the feedback gain on modes in the range $-2 \leq n \leq +2$ is zero and therefore no sidebands in the range of the tearing mode harmonics, the feedback results in improvement in the discharge. The time evolution for different modes is shown in the panel on the right-hand side of FIG. 1 for this targeted-mode case.

In FIG. 1 the direct effect of the targeted-mode feedback on the RWMs is evident and the growth of the RWM harmonics is in general reduced. Also there is an indirect effect in that the growth of the radial tearing-mode perturbation (n=-14) due to wall-locking is delayed when feedback is applied. There is an implication that the growth of RWM amplitudes can contribute to wall locking of rotating tearing modes through some nonlinear coupling mechanism. However it is also evident that the coupled modes n=-11 and n=+5, which are both RWMs, are not effectively stabilised. However it should be noted that with targeted mode feedback the time duration of the discharge can be extended from about 15 ms to about 25 ms.

According to the linear model, purely real gains are sufficient to stabilise non-rotating RWMs [5]. In FIG. 2 the grey areas qualitatively indicate values of gains (K_1, K_2), which can stabilise a pair of RWMs. The first case (light grey) refers to a case where only one of the modes in the pair is unstable, while in the second case (dark grey) both modes are unstable. We have assumed that in both cases the mode b_1 is the most unstable. If only one mode is unstable, the stabilisation can be achieved by feeding back only the signal of the unstable mode, K_1>0 and K_2=0, but other solutions are also possible if one would like to optimise the control. The simultaneous stabilisation of two unstable modes is more difficult, as shown by the smaller area of the stable region, and, moreover, requires negative values for the second gain (positive feedback), K_1>0 and K_2<0. Strategies with purely real gains have been shown to be very effective to control pairs of non-rotating modes where only one is unstable.

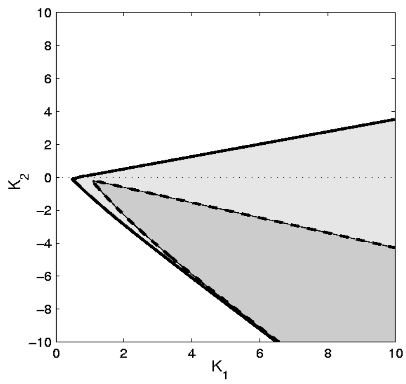

FIG. 2. Values of gains for coupled modes that result in stabilisation for the case with mode 1 unstable and mode 2 stable (light grey), and the case with both modes unstable (dark grey).

If one, or both RWMs in a pair are (slowly) rotating, a more efficient way to stabilise them involves complex gains, which allows synchronisation of the feedback action to the changing phase of the mode. Nonlinear simulations with feedback [6] have shown that complex gains can be used to control RWMs and that in this way the mode can be made to rotate. An example is shown in FIG. 3a, which displays a simulation in which the m=1, n=5 mode stabilization is achieved by changing the complex gain values. Correspondingly as seen in FIG. 3b, mode rotation is induced in different directions, depending mainly on the sign of the imaginary part of the gain.

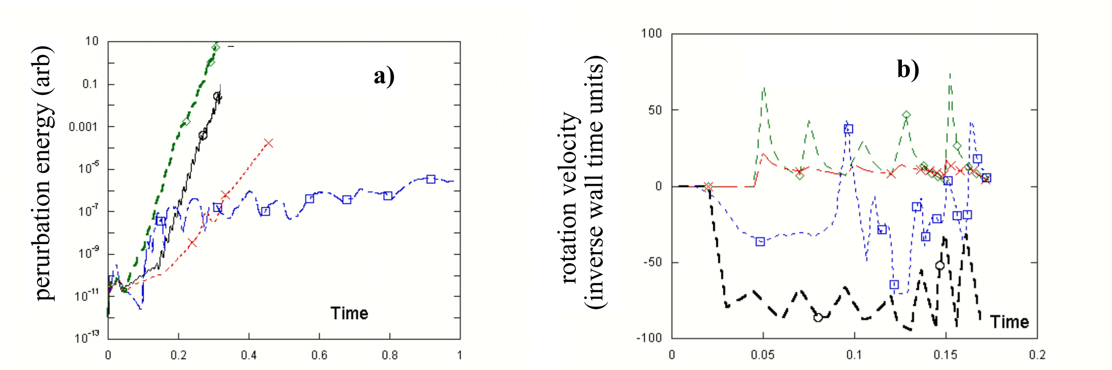

FIG. 3. In panels (a) and (b) code-simulation results are shown for the m=*1,* n=*5 mode for 4 different gains (black and blue lines have negative imaginary part) vs. time. Panel (b) shows the code-simulation rotation velocity (100 corresponds to 5 times the inverse wall penetration time). Time is in resistive diffusion time units (1 corresponds to around 15 wall times).*

The linear model has been used to analyze the feedback control of the coupled modes n=(5,-11), both slowly rotating. FIG. 4 shows the stability plot for this case. The contour lines indicate the real part of the most unstable pole of the system as a function of the imaginary part of the gains K_5 and K_{-11}, while the real part of the gains are fixed. With purely real gain the system is unstable, but the stable region, delineated by a bold black line, can be reached by increasing the imaginary parts, i.e., by following the dashed line.

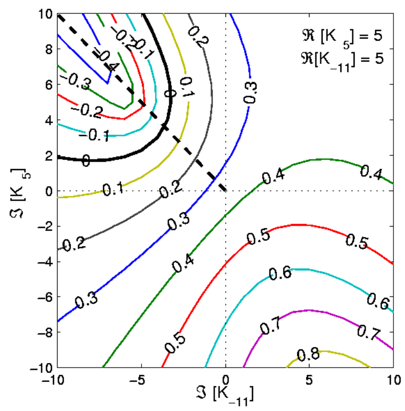

FIG. 4. Stability plot: real part of most unstable pole of the system as a function of the imaginary parts of the gains, with fixed real parts (gains have a different normalization than those shown in FIG. 5).

This strategy has been tested experimentally and has given some positive results as shown in FIG. 5. The coupled modes, n=+5 and n=-11 are shown for cases with different complex gains. The real part is fixed and the imaginary part is progressively increased. When real gains are used (green line) the n=+5 sideband is out of control. With complex gains the rotation speed (time derivative of phase) increases with increasing imaginary gain and both sidebands can be suppressed. However, the relatively short discharge (a few wall times) does not allow to completely verify the damped oscillatory behaviour predicted by the model.

In summary complex gains induce rotation and can contribute to feedback scenarios with reduced mode growth. Also for the case where there are sideband effects due to a discretization of the actuator saddle coils, complex gains can improve stability. However this effect cannot be reproduced by the nonlinear numerical code since an "idealized" continuous coil system is in place (no sidebands) in this case.

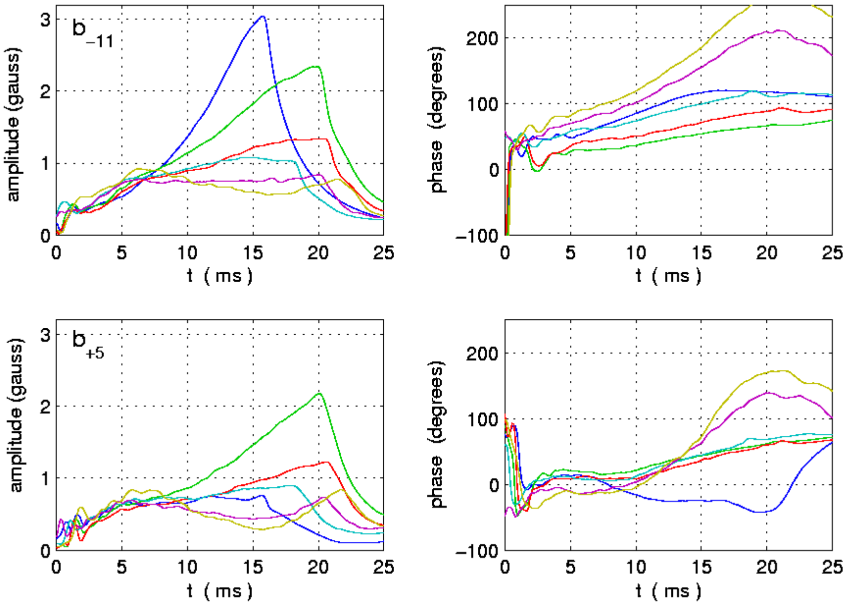

FIG. 5. Experimental measurements of the amplitude and phase for the n=(-11,+5) couple are shown. The reference case is blue. The complex gains are; green (K_{+5}=50+0i, K_{-11}=50+0i), red (K_{+5}=50+10i, K_{-11}=50-10i), cyan (K_{+5}=50+20i, K_{-11}=50-20i), magenta (K_{+5}=50+40i, K_{-11}=50-40i), yellow (K_{+5}=50+60i, K_{-11}=50-60i).

3. Resonant field error effects

It is evident in FIG. 1a that several modes have amplitudes exceeding that expected from unstable RWM growth at theoretical rates. The high amplitudes are attributed to externally-produced, resonant field error harmonics that affect the growth of these modes. The time dependence of a perturbation harmonic including the effect of an externally produced harmonic (which is also, of course, the basis for feedback control) has been described in a number of papers (see for example [7]). To compare the T2R experiment with theory, it is convenient to examine the time dependence of the radial field perturbation at the location of the sensor coils in the experiment. In the model for error field amplification by Pustovitov, [8], growth of a radial field harmonic n is given by;

$$\partial_t b_n = \gamma_{n,o} b_n + \gamma_{n,w} b_{n,ex}, \qquad (1)$$

where $b_n(t)$ is the perturbed field, $b_{n,ex}(t)$ is that part of $b_n(t)$ that is due to external sources (either a field error or a saddle-coil produced control harmonic or both), $\gamma_{n,o}$ is the natural growth rate of the plasma mode and $\gamma_{n,w}$ describes the diffusion rate of the harmonic at the thin wall, which is determined only by the mode numbers and wall parameters. The second term on the right-hand side of Eq. (1) describes perturbation growth due to field error amplification $b_{n,ex}(t)$ (for example when the field error is constant in time) even when the mode is marginally stable ($\gamma_{n,o}$=0).

The coefficient $\gamma_{n,w}$ in Eq. (1) is determined by estimating the characteristic wall diffusion time, $\tau_{w,n}=\gamma_{w,n}^{-1}$, of pre-programmed, pulsed perturbations with different helicity applied during vacuum shots. There is reasonably good agreement with the model prediction for a cylindrical continuous thin shell, as shown in FIG. 6. To obtain a good agreement for all the different harmonics, an effective diffusion time of about 5 ms for the $n=0$ harmonic has to be introduced, which is shorter than the measured vertical diffusion time (6 ms).

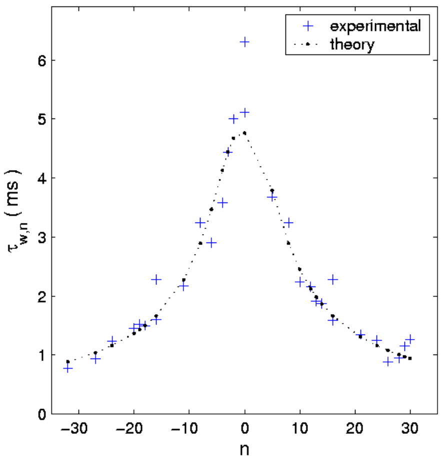

FIG. 6. Experimentally measured values for the magnetic field diffusion time of different (m=1,n) *harmonics and values calculated from the model (dashed line) are shown. Note the two experimental points for n=0 harmonic, for the diffusion time in the vertical and horizontal plane respectively.*

In Eq. (1) b_n and $b_{n,ex}$ are, in general, complex. However the phases of the natural RWMs are often constant during the discharge and reproducible from shot to shot. The reproducibility is attributed to the fact that reproducible field error harmonics, even at low levels, can establish the initial phase of the RWM. Because of the reproducibility, open loop experiments were performed where the controller/saddle coil array was used to generate a pre-programmed, pulsed, resonant control harmonic with the same phase as the natural plasma harmonic. Therefore the plasma and the resonant control perturbation can both be considered as real. Pre-programmed perturbations for three different harmonics have been applied to discharges to demonstrate the effect of the resonant field error-like perturbation. The time evolution of the perturbation, normalised to the equilibrium field, is shown in FIG. 7. In panel (a) the n=+10 mode is robustly stable, and the natural perturbation for this mode shows no sustained growth. The damping is sufficiently strong so that the field error effect is damped when the resonant control perturbation is applied during a plasma discharge. The resulting measured perturbation is essentially just the sum of the natural mode perturbation and the control perturbation. On the other hand the n=+5 mode, panel (b), is unstable and the natural perturbation amplitude grows during the pulse. When the resonant control perturbation is applied, the plasma response is an increase in the growth consistent with that due to the natural growth rate plus the field error induced growth effect as given on the right-hand side of Eq. (1). The third case shown is the n=-3 mode, panel (c), that is marginally unstable for most of the time interval shown, although at the end of the time interval, as the current decreases, the normalised mode amplitude increases. For this case, when the natural growth rate $\gamma_{-3,o}$ is approximately zero, the plasma response is perturbation growth due only to the field error effect. However the perturbation due to field error is not damped when the control perturbation decays toward zero. At the end of the time interval, the perturbation starts to grow, but from the higher level due to the effect of the field error.

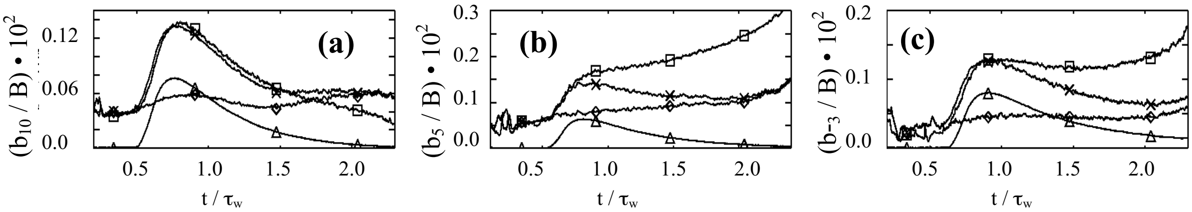

FIG. 7. Waveforms for the normalized, measured amplitudes of (a) n=+10 (stable), (b) n=+5 (unstable) and (c) n=-3 (marginally unstable) harmonics; (◊) the natural plasma harmonic without an external control field, (Δ) a pre-programmed, pulsed external control harmonic applied without plasma, (□) the harmonic with the same external control field applied to the plasma and (×) the calculated sum of the natural harmonic plus the control harmonic given as a reference for comparison to expose RFA effects.

The amplitude of the natural perturbation in FIG. 7 panel a) is about 0.05% of the equilibrium field and this is an indication of the magnitude of the natural field error for this harmonic.

4. Conclusion

Examples of active feedback control of RWMs have been experimentally demonstrated. The average mode amplitudes are reduced, and as a result of the suppression of modes, the discharges have been considerably prolonged in time. Mode rotation similar to that seen in nonlinear simulations and control of sidebands have been demonstrated using complex gains. Also open-loop experiments have shown that resonant field error effects are present in the system and must be taken into account.

[1] C.G. GIMBLETT, "On free boundary instabilities induced by a resitive wall", Nuc. Fusion **26** (1986) 617.

[2] P.R. BRUNSELL, *et al.*, "Initial results from the rebuilt EXTRAP T2R RFP device", Plasma Phys. and Contr. Fusion **31** (2001) 1457.

[3] P.R. BRUNSELL, *et al.*, "Resistive wall modes in the EXTRAP T2R reversed-field pinch", Phys. of Plasmas **10** (2003) 3823.

[4] M. CAVINATO, et al, "Comparison of strategies and regulator design for active control of MHD modes", 23rd Symposium on Fusion Technology, 20-24 September 2004, Venice Italy, Paper P3C-C-377.

[5] R. PACCAGNELLA, *et al.*, "Feedback control of resistive wall modes in reversed field pinches", Nuclear Fusion **42** (2002) 1102.

[6] R. PACCAGNELLA, *et al.*, "Feedback studies on RWMs in the RFP", Phys of Plasmas **9** (2002) 234.

[7] R. FITZPATRICK and E.P. Yu, "Feedback stabilization of resistive wall modes in a reversed-field pinch", Phys Plasmas **6** (1999) 3536.

[8] V.D. PUSTOVITOV, Error field amplification near the stability boundary of the modes interacting with a conducting wall", Fizika Plazmy **30** (2004) 211.